

# The new MRTOF spectrograph for nuclear masses following RIBF's ZeroDegree spectrometer, featuring new methodologies for ion selection and mirror optimization

M. Rosenbusch,<sup>1</sup> M. Wada,<sup>1</sup> S. Chen,<sup>2</sup> A. Takamine,<sup>3</sup> S. Iimura,<sup>3,4</sup> D. Hou,<sup>5,6,7</sup> W. Xian,<sup>2</sup> S. Yan,<sup>8</sup> P. Schury,<sup>1</sup> Y. Ito,<sup>9</sup> H. Ishiyama,<sup>3</sup> S. Kimura,<sup>3</sup> J. Lee,<sup>2</sup> J. Liu,<sup>2</sup> S. Michimasa,<sup>10</sup> H. Miyatake,<sup>1</sup> J. Y. Moon,<sup>11,12</sup> S. Nishimura,<sup>3</sup> S. Naimi,<sup>3</sup> T. Niwase,<sup>3,12</sup> and H. Wollnik<sup>13</sup>

<sup>1</sup>*Wako Nuclear Science Center (WNSC), Institute of Particle and Nuclear Studies (IPNS), High Energy Accelerator Research Organization (KEK), Wako, Saitama 351-0198, Japan*

<sup>2</sup>*Department of Physics, The University of Hong Kong, Pokfulam, China*

<sup>3</sup>*RIKEN Nishina Center for Accelerator-Based Science, Wako, Saitama 351-0198, Japan*

<sup>4</sup>*Department of Physics, Graduate School of Science, Osaka University, 1-1 Machikaneyama, Toyonaka, Osaka 560-0043, Japan*

<sup>5</sup>*Institute of Modern Physics, Chinese Academy of Sciences, Lanzhou 730000, China*

<sup>6</sup>*University of Chinese Academy of Sciences, Beijing 100049, China*

<sup>7</sup>*School of Nuclear Science and Technology, Lanzhou University, Lanzhou 730000, China*

<sup>8</sup>*Institute of Mass Spectrometry and Atmospheric Environment, Jinan University, Guangzhou 510632, China*

<sup>9</sup>*Advanced Science Research Center, Japan Atomic Energy Agency, Ibaraki 319-1195, Japan*

<sup>10</sup>*Center of Nuclear Study (CNS), The University of Tokyo, Bunkyo 113-0033, Japan*

<sup>11</sup>*Institute for Basic Science, 70, Yuseong-daero 1689-gil, Yuseong-gu, Daejeon 305-811, Korea*

<sup>12</sup>*Kyushu University, Hakozaki, Higashi-ku, Fukuoka 812-8581, Japan*

<sup>13</sup>*New Mexico State University, Las Cruces, NM 88001, USA*

(Dated: October 25, 2021)

A newly assembled multi-reflection time-of-flight mass spectrograph at RIKEN's RIBF facility became operational in spring 2020, and first optimization procedures and performance tests using stable ions have been completed. As the capability to study nuclear isomers by mass separation is essential for modern nuclear mass studies, a useful optimization scheme has been developed to tackle the multi-parameter problem of the electrostatic mirror voltages enabling a narrow time-of-flight focus. To this end the average kinetic energy of the ions during the reflection period has been varied within a wide range of about  $\Delta E_{\text{kin}} = 200 \text{ eV}$ , which allows simplified measurements of the characteristic energy dispersion function of the device. This serves as a well-distinguishable response to changes of the mirror potentials rather than observation of time-of-flight focal width only. Presently, a mass resolving power of  $R_m > 1\,000\,000$  has been reached within a total time-of-flight of only 12.5 ms making the spectrometer capable of studying nuclei with low-lying nuclear isomers. Other technological novelties of this state-of-the-art setup are in-MRTOF ion selection methods to separate molecular contaminants from the ions of interest, which will be introduced. The setup underwent an initial online commissioning at the BigRIPS facility in the end of 2020 where more than 70 nuclear masses have been measured with high precision and accuracy.

## I. INTRODUCTION

Continuing advances for multi-reflection time-of-flight mass spectrographs (MRTOF-MS) play a vital role for fast and precise measurements of short-lived exotic nuclides produced at radioactive ion beam (RIB) online facilities worldwide. From its invention [1] onwards, every new step in the development of MRTOF-MS technology has given new advantages, such as the resolution and separation of isobars [2–4] and isomeric nuclear states [5], and the precise measurement of previously unknown nuclear masses [6–12]. A strong point is the short duration of the measurement required to enable mass resolving powers of  $R = \frac{m}{\Delta m} = \frac{t}{\Delta t} > 100\,000$ , where  $m$  and  $t$  are the ion mass and time-of-flight (TOF) while  $\Delta m$  and  $\Delta t$  are the full widths at half maximum (FWHM) of mass and the TOF spectral peaks, respectively. This duration is on the order of ten milliseconds, occasionally extending to a few tens of milliseconds. Presently various research groups around the world are taking part in the development of MRTOF systems at RIB facilities,

including RIKEN (Japan) [13, 14], CERN/ISOLDE (Switzerland) [2, 6], GSI (Germany) [15, 16], TRIUMF (Canada) [11, 17], Argonne (USA) [18], Notre Dame University (USA) [19], GANIL (France) [20], IMP (China) [21], and JYFL (Finland). Apart from these applications, MRTOF technology has advanced to other research fields including fundamental neutrino physics, where the focus is on unambiguous identifications of rare events [22].

A new state-of-the-art MRTOF apparatus [23] called ZeroDegree-MRTOF (ZD-MRTOF) system has become operational at the BigRIPS facility of RIKEN, where exotic nuclei can be produced with high yield [24, 25]. This system was coupled to a cryogenic helium filled gas cell located behind the ZeroDegree spectrometer (see [26] for the ZD spectrometer) to slow down the initially high-energy reaction products from relativistic energies to thermal equilibrium with the helium gas, and perform high-precision mass measurements of the exotic atomic nuclei. Herein we introduce the new system with its associated technical advances.

The basic principle of MRTOF-MS is the repetitive re-

flection of ions between two (typically concentric) electrostatic ion mirrors with the aim to focus ions to a TOF detector with a TOF distribution as narrow as possible after their long flight path. To this end the ion-optical aberrations must be minimized, where one of the crucial ingredients for MRTOF systems is the distribution of mirror voltages forming a characteristic shape. On one hand, these electric potentials are optimized to keep radial ion-optical aberrations small, which intuitively means that the radial expansion of the ion beam is kept as small as possible at all positions to approach a one-dimensional system. One important development in this context was the introduction of strongly negative voltages at certain positions in the system (negative ion-optical lens) [27], which also serves for radial confinement in general. On the other hand the voltage distribution is the generator for the TOF-energy dispersion function (see, *e.g.* [28]), which determines the relation between the kinetic energy of an ion and the final time-of-flight:  $\text{TOF}(E_{\text{kin}})$ . This function has been taken into account for the optimization of mirror electrodes in this work, and the correction of  $\text{TOF}(E_{\text{kin}})$  yielded a useful initialization to reach high resolving powers.

Another important issue is the difficult challenge coming from the propensity for the stable molecules in the gas cell to be ionized, either directly by interaction with the energetic beam or in secondary reactions with the ionized helium. When these stable molecular ions have a sufficiently similar mass-to-charge ratios  $A/q$  (with  $A$  being the atomic mass number and  $q$  the ions' electric charge) to the radioactive ions being analyzed, they can be useful internal references. However, when  $A/q$  is sufficiently differing from that of the radioactive ions then they will reach the detector after performing a different number of laps inside the MRTOF-MS, which leads to an unwanted overlapping of TOF signals and hinders the unambiguous identification of the wanted ion species. To solve such problems, a growing trend not only for nuclear physics but also for analytical chemistry [29] is the in-MRTOF separation of ions, *i.e.* removing unwanted ions during the reflection period in the MRTOF-MS. The most prominent method is the application of a deflection device in the MRTOF-MS first done for molecular studies [30] and was later adopted for the research on exotic nuclei [31] and, more recently, studied with an MRTOF setup for atomic clusters [32]. An alternative approach has been introduced from analytical chemistry, where the mirror endcaps of an MRTOF-MS have been repetitively opened shortly for ion separation [29]. Furthermore, a scheme using a single voltage pulse for the central drift tube of an MRTOF-MS was presented for the separation of isobaric contaminants [33]. We introduce a new method for wideband in-MRTOF ion separation, concentric-geometry in-MRTOF separation (CGIMS), based on repeatedly pulsing the mirror electrodes close to the central drift tube of the device.

In this work, the new setup along with geometry and applied voltages will be presented and the new in-

MRTOF ion separation scheme introduced. This is followed by a discussion of the optimization of mirror electrode voltages by measuring TOF-energy functions using a pulsed drift tube to change the ions' mean kinetic energy. In the end, we further discuss an on-line measurement commissioning using parasitic beam from in-beam  $\gamma$ -ray experiments (see *e.g.* [34]) in the end of 2020, where more than 70 nuclear masses were measured with high precision and accuracy.

## II. EXPERIMENTAL SETUP

The new device has a similar design and operation to the setup reported in [35]. In the following the present electrode configuration and the applied voltages will be shown. Furthermore, the in-MRTOF cleaning technology CGIMS will be introduced and contrasted with the use of an in-MRTOF deflector. The vacuum system and the experimental timing sequence will be discussed as well.

### A. Electrode Setup and applied Voltages

The new mass-measurement setup is dedicated to high-precision nuclear mass measurements at the BigRIPS on-line facility of RIKEN in Japan. The new spectrometer has been coupled to a novel helium-gas-filled ion catcher [36, 37] (see also, *e.g.* [38–42]) where relativistic radioactive ions are stopped, extracted and transported to the MRTOF system. For off-line studies and optimization of experimental parameters, an independent alkali ion source is used. It also serves as a source of reference ions for high-precision mass measurements when the device is operated on-line. Ions are continuously injected into a linear Paul-trap for accumulation and bunching, transported to a planar Paul trap referred to as flat ion trap (FT) for further collisional cooling in a dilute helium environment. The cooled ions are perpendicularly ejected from the flat ion trap and accelerated into a transfer section which connects the MRTOF-MS with the Paul traps. After passing a steering unit, a pulsed drift tube can be used to adapt the ions' energy. It is followed by another drift section before the ions enter the MRTOF device. The ions are trapped by fast switching of the first mirror electrode's bias (injection endcap). They are reflected back and forth for a chosen number of laps before being released by fast switching of the final mirror electrode's bias (ejection endcap). After exiting the MRTOF-MS, ions travel to a fast ion impact detector (MagneToF from ETP) and the time from their ejection from the flat ion trap to their impact on the MagneToF detector is digitized with a 100 ps precision multi-hit time-to-digital converter (MCS6 from Fast ComTech).

The present electrode design of the MRTOF-MS setup is shown in Fig. 1 (adapted from Fig. 1 in [23]). Ions from the gas cell or from the alkali ion source are simultaneously injected as a continuous beam into their adjacent

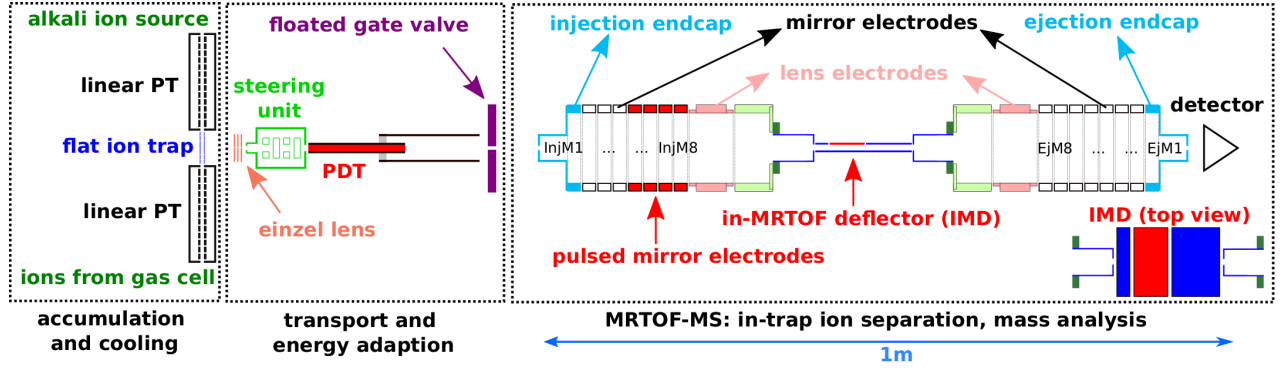


FIG. 1. Electrode configuration of the present MRTOF setup. Red color is chosen for electrodes pulsed for manipulation of the ions' energy, and for ion deflection.

segmented linear Paul trap and are then alternately forwarded to the central flat ion trap as a discrete ion bunch via fast switching of the trap DC potentials. The alternating injection of ions into the central trap from either source, gas cell or reference ion source, changes cycle by cycle to enable the concomitant referencing technique [43]. The flat ion trap, being the final stage of ion preparation, is used for additional cooling (without further accumulation of ions) and for properly locating the ion cloud to prepare the perpendicular ejection towards the MRTOF device through a small exit aperture of 0.7 mm diameter.

An accelerating einzel lens composed of three plates, each having an aperture of 3 mm, is used to provide spatial focusing while accelerating the ions to  $E_{\text{kin}} \approx 1.4 \text{ keV}/q$ . Beyond the third plate the ions pass a double steerer unit, which is floated on the potential of the third plate of the einzel lens. The deflector section is followed by the pulsed drift tube (15 cm in length and 1.5 cm in diameter) the bias of which, during the ions' passage, is rapidly increased from  $V_{\text{PDT-low}} = -1.4 \text{ kV}$  to about  $V_{\text{PDT-high}} = +1.1 \text{ kV}$  without disturbing the trajectory of the ions. This allows to adjust the ions' energy and to keep the potential of the center part of the MRTOF-MS ( $V_{\text{M-drift}}$ ) at ground potential, while also the flat ion trap is close to ground potential.

The ions exit the pulsed drift tube and enter a static drift tube of larger diameter (see also next section) which is floated to the same voltage  $V_{\text{drift}} = V_{\text{PDT-high}}$ . In this configuration the ions move field free for a distance of about 30 cm until reaching the entrance of the MRTOF device.

The presently applied approximate voltages for the ion-transfer and MRTOF-MS are given in Tab. I together with the relative sensitivity coefficients  $C_i = \frac{\delta \text{TOF}_i / \text{TOF}}{\delta V_i / V}$  of the mirror electrodes, where  $\delta \text{TOF}_i$  is the change of the TOF induced by the change  $\delta V_i$  in voltage.

The MRTOF mirror setup consists of eight electrostatic mirror electrodes and one (longer) electrode intended as ion optical lens on each side of the electrically grounded central drift tube (see [23] for geomet-

TABLE I. List of approximate voltages used for ion transfer from the flat ion trap to the MRTOF device. Electrode name, voltage, sensitivity coefficient (only for voltages used in reflection mode), and description.

name	voltage	$C_i$	description
$V_{\text{FT}}$	-10 V	—	center of FT
$V_{\text{Eje+}}$	+190 V	—	FT positive ejection
$V_{\text{Eje-}}$	-210 V	—	FT negative ejection
$V_{\text{A1}}$	-300 V	—	first acceleration plate
$V_{\text{A2}}$	-320 V	—	second acceleration plate
$V_{\text{A3}}$	-1400 V	—	third acceleration plate
$V_{\text{Def}}$	-1400 V	—	deflector section floating
$V_{\text{PDT-low}}$	-1400 V	—	pulsed drift tube low
$V_{\text{PDT-high}}$	+1100 V	—	pulsed drift tube high
$V_{\text{drift}}$	+1100 V	—	static drift tube
$V_{\text{valve}}$	+1100 V	—	float gate valve
$V_{\text{InjM1-op}}$	+1230 V	—	open mirror 1 injection side
$V_{\text{InjM1-cl}}$	+3080 V	-24.49 %	closed mirror 1 injection side
$V_{\text{InjM2}}$	+2220 V	-3.17 %	mirror 2 injection side
$V_{\text{InjM3}}$	+2540 V	+0.65 %	mirror 3 injection side
$V_{\text{InjM4...8}}$	0 V	—	mirrors grounded
$V_{\text{InjL}}$	0 V	—	lens grounded
$V_{\text{M-drift}}$	0 V	—	drift tube grounded
$V_{\text{EjL}}$	-4890 V	-3.63 %	lens ejection side
$V_{\text{EjM7,8}}$	+900 V	+1.28 %	mirror 7,8 ejection side
$V_{\text{EjM6}}$	+1030 V	+1.98 %	mirror 6 ejection side
$V_{\text{EjM5}}$	+2950 V	+8.00 %	mirror 5 ejection side
$V_{\text{EjM4}}$	+1320 V	+2.54 %	mirror 4 ejection side
$V_{\text{EjM3}}$	+2603 V	-5.01 %	mirror 3 ejection side
$V_{\text{EjM2}}$	+2260 V	-8.92 %	mirror 2 ejection side
$V_{\text{EjM1-cl}}$	+3500 V	-19.37 %	closed mirror 1 ejection side
$V_{\text{EjM1-op}}$	+500 V	—	open mirror 1 ejection side

ric details). Both injection and ejection of ions is enabled by switching the potentials of the outermost electrodes at the injection- and ejection side mirror endcaps to a potential at which the ions, having a kinetic energy close to  $2.5 \text{ keV}/q$ , can pass at the appropriate moment (high-voltage switching by in-house built fast transistor switches). The ion TOF detector is located about 5 mm away from the ejection endcap electrode.

The voltage configuration in the MRTOF-MS is an asymmetric pattern where only three mirrors are used

on the injection side to form a steep potential well, while all other electrodes up to the lens of the injection side are usually grounded. At the ejection side, all mirror electrodes are used to form a shallow shape which allows for manipulation of the ions' position-energy distribution so that a time focus can be achieved after the anticipated number of laps. All mirror voltages are applied through low-pass filters with 1 – 2 s time constant for the most inner mirrors with lower voltage (1 M $\Omega$ , 1 – 2  $\mu$ F), 5 s time constant for  $V_{\text{EjM}2,3,4,5}$  (5 M $\Omega$ , 1  $\mu$ F), and 40 s time constant for the most outer mirrors  $V_{\text{InjM}1-\text{cl}}$  and  $V_{\text{EjM}1-\text{cl}}$  (5 M $\Omega$ , 8  $\mu$ F).

The application of low-pass filters supports the stabilization of voltages, but also bring drawbacks for the usage of switched mirrors. During continuous switching of voltages, electric charges are transferred between the two applied capacitors (*i.e.* open and closed state of an ion mirror). As there are large resistors separating the capacitor from the input channel, the resulting voltage at the electrode depends on the switching frequency. The current through the resistor is defined by the average charge load, but also by the voltage difference between the input of the filter and the electrode after the filter. Thus the timing system has been prepared to allow for an interruption-free reprogramming (see Section IID). A further active voltage stabilization as in earlier setups of this group [14], and developed in other groups in parallel [44, 45] (and presently being renewed for future use [46]), is anticipated at the ZD MRTOF setup for the future.

Using the sensitivity coefficients, the mass resolving power  $R_m$  which can be achieved after considering voltage fluctuations is given by

$$R_m = \frac{1}{2} \frac{TOF}{\Delta TOF_{\text{ion}} + TOF \cdot \sqrt{\sum_i (C_i \cdot (\delta V/V)_i)^2}}, \quad (1)$$

where  $(\delta V/V)_i$  is the relative voltage noise for each electrode. Dominant contribution comes from the most outer mirror electrodes and yields a requirement, for example, of an average voltage fluctuation of  $\delta V/V \approx 1.4 \cdot 10^{-6}$  to reach  $R_m \approx 10^6$  if the intrinsic ion distribution is not considered, and  $\delta V/V < 10^{-6}$  in a realistic case. This denotes the minimum relative stability which must persist for a time interval within which a reference spectrum of sufficient statistics is obtained to accommodate software correction.

## B. In-MRTOF ion separation and the alternative method CGIMS

A challenge for the new setup is the delivery of contaminant molecules with different mass-to-charge ratios. These molecules are ionized in the gas cell by the incoming high-energy ion beam. This leads to the dominant presence of ions with different lap times in the MRTOF-MS and the subsequent detection of TOF peaks with unknown number of laps overlapping with the ions of interest in the same spectrum. Hence, a separation of all

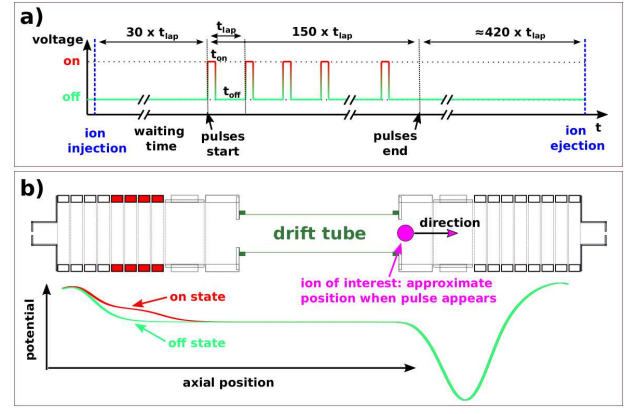


FIG. 2. Illustration of the CGIMS scheme. a) Pulse timing structure: pulses are synchronized to the motion of the wanted ion species during the ion trapping period, where  $t_{\text{lap}}$  is the lap time of the ions of interest and  $t_{\text{on}}$  ( $t_{\text{off}}$ ) is the on (off) state duration of the pulse in each lap. b) Potential shape for on/off state of the 600 V pulse and position of the wanted ion species at start of the  $t_{\text{on}}$  time.

contaminant non-isobaric ions is essential for the success of online experiments.

During the first online commissioning of the setup in 2020 (see results in Sec. IV) a concentric-geometry in-MRTOF separation (CGIMS) scheme has been developed as a new alternative methodology for in-MRTOF ion separation (see Fig. 2). Initially, the measurement of exotic species was hindered by the high amount of contaminant molecules delivered from the gas cell, and at the time of the experiment a deflector unit inside the MRTOF-MS was not installed. To nonetheless succeed the measurement, the four (otherwise grounded) mirror electrodes indicated by red color in Fig. 1 and 2, have been used to provide strong periodically pulsed potential variations of concentric geometry within the vicinity of these electrodes. This acts similar to a pulsed drift tube and causes a violation of the kinetic energy for ions present in the affected region during the increasing or decreasing slope of the electric pulses. The energy can be increased or decreased depending on the polarity of the voltage transition.

The pulses were introduced by a fast transistor switch altering the potential between the electrical ground of the system and a voltage supply adjusted to about +600 V. As the electric pulses propagating through the system can induce a disturbance on other electrodes, the chosen voltage was a compromise between sufficiently ejecting the unwanted ions and maintaining high accuracy for the mass measurement of isobaric chains. The pulses were synchronized with the lap time of the ions of interest so that the location of desired ion species was in a non-affected region when the pulse was present.

As an ejection from the system is not achieved by crossing the region while the high voltage is static, the unwanted molecular ions must occasionally cross the region and experience the voltage transition once or sev-



eral times until they were ejected from the system. The success of ion ejection depends on the position of the unwanted ions during the voltage transition and, if not ejected, several pulses are needed. A satisfying performance was reached by using a larger number of pulses, *i.e.* 150 pulses in equally many subsequent laps (total number of laps for wanted ions species was mostly 600 during the experiments), with a duration of  $3 - 5 \mu\text{s}$  for each pulse. Before starting the CGIMS pulses after ion injection into the MRTOF-MS, a waiting period of about 30 laps was applied to provide time for spatial ion separation. This separation scheme was successful and the resulting TOF spectra were sufficiently clean to measure the rare species delivered from the beam facility. In Fig. 3 the measurement of  $A/q = 86$  isobars is shown with and without the application of the new cleaning method. In the top, only two dominant peaks from the bottom spectrum would be recognizable, but even so it would not be known if other ions are not overlapping with the ions of interest. The unambiguous identification of the ion species would not be possible without the application of an in-MRTOF separation scheme. This cleaning scheme is presently being further investigated by simulations.

Another scheme coming into question was introduced in [29]. In this study a well-timed short opening of the mirror endcap electrodes was used for mass selective ion ejection from an MRTOF-MS. While such a scheme has a good performance in guaranteeing ion ejection, it has the drawback that high-precision mass measurements performed in the same device during the same trapping period is challenging due to the voltage dynamics at the ion mirrors.

A further method for ion separation has been studied at CERN/ISOLDE and concentrates on isobaric separation by a single pulse applied to the central drift tube of an MRTOF-MS [33] during ion ejection with the in-trap lift method [28]. It is a narrow-band separation method specialized for isobaric contaminants, where a wideband ion separation with such methodology would require multiple pulses during the trapping period.

The presently most promising technique to provide the desired separation is the use of a deflection device located inside the MRTOF-MS [30–32], which we refer to as in-MRTOF deflector (IMD). A new prototype of in-MRTOF deflector with a planar geometry has recently been installed in the central drift region of the ZD-MRTOF system and is presently studied in off-line experiments. Two stainless steel plates are placed in a distance of 1 cm, where one of them is separated to host a pulsed 5 cm long electrode enabling the deflection of ions. The lateral width of all plates is 10 cm to provide sufficient electric shielding of the area. By the choice of plate distance and size, a single hit with a dipole field of only 30 V/cm is necessary to cause an ejection of unwanted ions within the same lap, *i.e.* before they can exit the IMD section. This allows for a targeted selective ejection at chosen lap numbers and, thus, for a selective maintaining of ions with different  $A/q$  while ejecting all other ions.

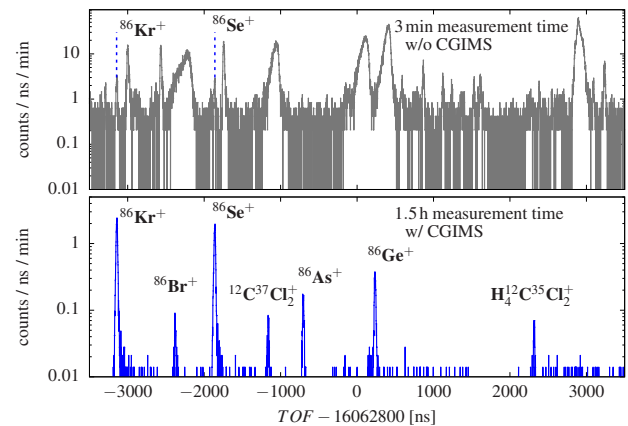


FIG. 3. On-line application of in-MRTOF cleaning using electric pulses applied to four mirror electrodes. Two spectra of  $A/q = 86$  ions delivered from the BigRIPS facility have been recorded. In the top the cleaning method is not applied and molecular contaminants of other masses performing different numbers of laps in the MRTOF-MS are present throughout the TOF spectrum. In the bottom, the purified spectrum is shown, where only species with  $A/q = 86$  are remaining.

### C. Vacuum setup

The vacuum system (see Fig. 4) is optimized to allow for sufficient helium gas pressure in the Paul traps while preserving ultra-high vacuum inside the MRTOF chamber, and while keeping the length of the transfer section moderately short. To this end the linear Paul traps are fully encapsulated by thin metal tubes being also a part of the mounting structure for them. The tubes further reach inside the holder of the flat ion trap and provide full sealing towards the outer trap chamber. The circuit boards with the electrode structure of the flat ion trap are glued to the holder so that the linear Paul traps and the flat ion trap are a closed volume referred to as inner trap chamber. Helium gas is injected directly into the flat ion trap using an access port at the trap holder, which also supplies the linear Paul traps. The only leakage to the outer trap chamber is due to the necessary 0.7 mm aperture for ion ejection. The inner and outer trap chamber are separately pumped by turbomolecular pumps (TMP), which provides the first two essential pumping stages (Edwards STP-451, and Edwards STP-H451C).

The next pumping barrier towards the MRTOF device is enabled by the design of the outer trap chamber. The steerer unit is installed into a cylindrical housing to seal the outer trap chamber towards the subsequent ion transfer section. The aperture at the entrance of the steerer section has a 6 mm diameter, and at the exit the pulsed drift tube is mounted having a length of 150 mm with 15 mm diameter. These two units provide a second pumping barrier.

The transfer section is separately pumped by TMP (SEIKO SEKI STP-301) with independent pre-pump and

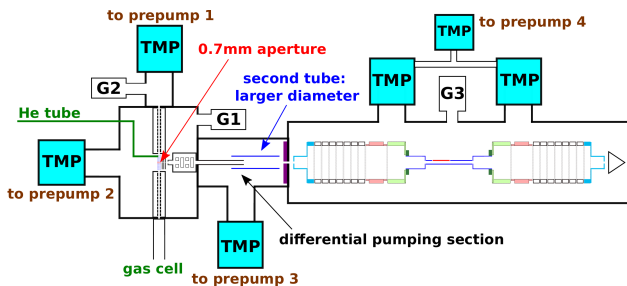


FIG. 4. Sketch of the vacuum system with three differential pumping stages to reduce the helium load in the MRTOF-MS. The symbols G1,G2,G3 denote vacuum gauges.

the adjacent tube to the pulsed drift tube has a larger diameter to allow for sufficient gas flow to the TMP. The third and last pumping barrier towards the MRTOF chamber is the 6 mm aperture at the gate valve in open state. The chamber of the mass analyzer is pumped by two TMPs in parallel (Edwards STP-451), of which the back ends are further pumped by a smaller TMP (Edwards NEXT85D) to provide more efficient pumping by a low-pressure back end. This vacuum configuration allows presently for about  $3 \cdot 10^{-6}$  Pa caused by the helium stream into the MRTOF chamber (outer trap chamber with gauge G1:  $2 \cdot 10^{-2}$  Pa), while the pressure inside the flat ion trap is estimated to be on the order of 1 Pa (no vacuum gauge inside the trap). Despite the additional efforts, some of the residual helium gas in the MRTOF-MS causes unwanted ejections of ions from the MRTOF system with increasing flight path of ions. As shown in Fig. 5, the transmission of singly-charged  $^{39}\text{K}^+$  ions over the course of 1200 laps is measured to be about 70 % while the flight path is on the order of 2 km and the time of flight 21 ms. Usual operation is done with lap numbers between 500 and 700 where about 80 % of the potassium ions have been transmitted. The estimated mean free path is about 5 km.

#### D. Measurement Sequence

As described in [43], both linear Paul traps are usually filled with ions independently (and simultaneously) from each source: the reference ion source and the on-line helium gas catcher. Both of the linear Paul traps transfer ions alternately to the central flat ion trap, where the ions are cooled and then ejected towards the MRTOF system. Except for the short moment of transfer to the flat ion trap, both linear Paul traps are continuously in accumulation and cooling mode (axial trapping potential depth is on the order of  $-10$  V). While one of the linear trap injects ions into the central trap the potential of the other linear trap is in fully closed (accumulation and trapping) mode, where the potential of the segment closest to the flat ion trap is a reflecting well. This alternate injection enables the concomitant refer-

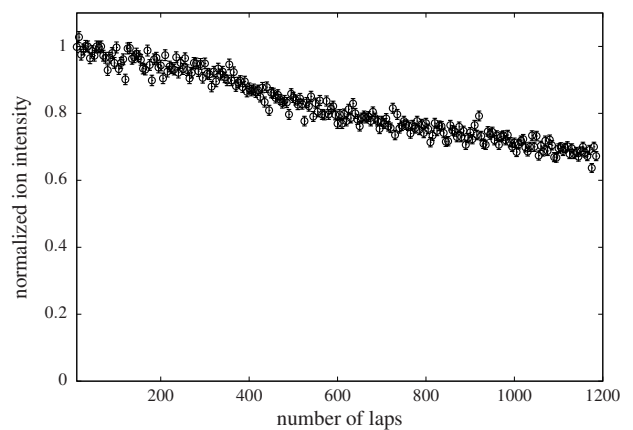


FIG. 5. Normalized ion intensity of  $^{39}\text{K}^+$  ions as a function of the number of laps performed in the MRTOF-MS. At the highest investigated lap number the ions' flight path is 2.2 km while each lap has a flight path of approximately 1.8 m. The corresponding TOF for this  $A/q$  is on the order of 20 ms.

encing method [10, 43] which allows for highly frequent measurements of reference ions (at present every 50 ms) and thus for excellent compensation of TOF drifts mainly caused by voltage fluctuations and thermal expansion of the mechanical structure.

The full measurement sequence consists of two subcycles (presently of 25 ms length) including the injection of ions from either of the linear Paul traps into the flat ion trap, cooling of ions, ejection towards the MRTOF-MS, and trapping period in the MRTOF system. The interleaved timing sequence is shown in fig. 6, where each second TOF measurement cycle contains the same type of ions, either from the reference source or from the gas-filled ion catcher. Except for the alternate injection of ions into the flat ion trap the timing patterns for both ion species are similar: cooling in the flat ion trap, ejection from this trap, adapting the energy with the pulsed drift tube switched at appropriate moment when the ions are well inside the tube, closing the injection mirror after the ions passed, and opening the ejection mirror when the ions have performed the desired number of laps in the MRTOF-MS. The timings for the pulsed drift tube and both mirrors are mass dependent, where the trigger signals for the high-voltage transistor switches are provided by an in-house built FPGA sequencer. To avoid voltage instabilities for the switched high-voltage electrodes connected to low-pass filters via keeping a constant load between the two voltage inputs, the cycle is running continuously and independent of data recording. When parameters are changed the FPGA system is reprogrammed during operation and does not stop the output of trigger signals before changing the timing pattern.

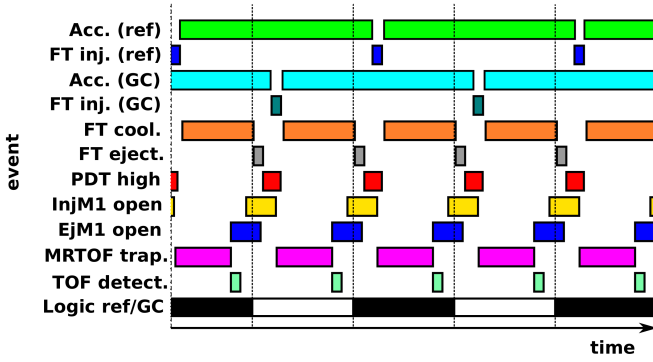


FIG. 6. Interleaved event scheme of the measurement sequence. **Acc. (ref)**: Accumulation and cooling of ions in reference Paul trap ( $\approx 40$  ms). **FT inj. (ref)**: Injection of ions from the reference trap into flat ion trap (few microseconds). **Acc. (GC)**: Accumulation of ions in the Paul trap adjacent to the gas cell ( $\approx 40$  ms). **FT inj. (GC)**: Injection of ions from gas-cell side Paul trap into flat ion trap (few microseconds). **FT cool.**: Cooling of ions in flat ion trap (2 – 7 ms). **FT eject.**: Ejection of ions towards the MRTOF section. **PDT high**: Pulsed drift tube at  $V_{\text{PDT-high}}$  ( $V_{\text{PDT-low}}$  otherwise). **InjM1 open**: Injection endcap at open state (closed otherwise). **EjM1 open**: Ejection endcap open state. **MRTOF trap.**: Symbolic for reflection period in MRTOF system. **TOF detect.**: TOF detection (typically 10 – 20 ms TOF). **Logic ref/GC**: Logic tag signal for data acquisition. See [43] for an alternative illustration.

### III. ION MIRROR OPTIMIZATION AND OFF-LINE PERFORMANCE

The goal of the optimization of the mirror potentials is to achieve a narrow time distribution of ions at the TOF detector, which in turn means that (beside other ion-optical aberrations) different kinetic energies created by different starting positions in the preparation Paul trap must be compensated to achieve the same time-of-flight for all energies imprinted on the ions by the extraction field. The extraction field forms the initial correlated position-energy distribution within the ion cloud, which is converted into a TOF distribution at the detector (see Fig. 18 and 19 of [47] for analog spatial imaging in sector magnet spectrometers). This distribution  $\text{TOF}(E_{\text{kin}})$  is nonlinear in general and depends on all ion optical elements in the system. As a major effort for the optimization, this distribution has to be compensated by the potential shape of the ion mirrors to obtain a high quality time focus. The lowest limit achievable in theory is that of the ions' turnaround time due to the unavoidable finite thermal energy distribution in the ion trap, which is the uncorrelated part of the initial position-energy profile of the ion cloud.

As the mirror electrodes create a multi-parameter system, a particular challenge comes up to find the best voltage combination. An additional obstacle present for mass spectrometry of rare ions is that the phase space of the ions from the preparation trap cannot be cut (*e.g.*

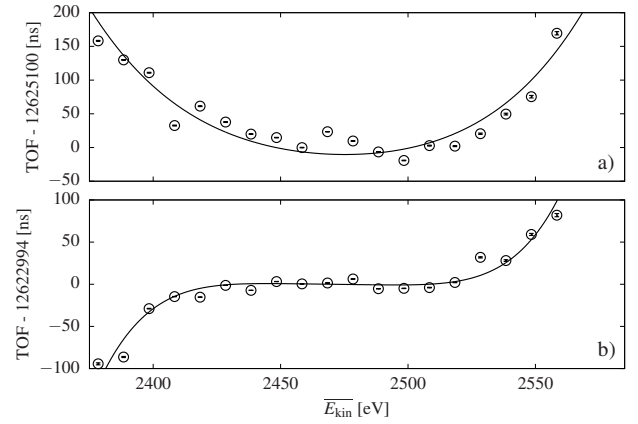


FIG. 7. a) Time-of-flight of  $^{39}\text{K}^+$  ions as a function of the mean kinetic energy varied by the electric potential  $V_{\text{PDT-low}}$  of the negative (entrance) voltage of the pulsed drift tube for a detuned mirror potential allowing isochronous behavior only for a small energy interval. b) Same measurement for well-tuned mirror potentials showing a significantly larger isochronous energy interval.

by a beam collimator) to increase the resolving power, as this would include a loss of valuable events. Thus, the problem must be solved entirely by ion optics and stable voltages.

While also in the present work the mirror voltages were ultimately tuned one by one during repeated measurements of the mass resolving power, the pulsed drift tube was additionally applied to achieve a useful overview about the  $\text{TOF}(E_{\text{kin}})$  dispersion distribution, as a preparatory step of the final optimization. In order to modify the kinetic energies, ions ( $^{39}\text{K}^+$ ) were accelerated into the pulsed drift tube at different electric potentials  $V_{\text{PDT-low}}$ , whereas the post-pulse voltage  $V_{\text{PDT-high}}$  was not changed. The ions were then stored in the MRTOF-MS for 690 laps and ejected towards the TOF detector. The dispersion distribution  $\text{TOF}(E_{\text{kin}})$  can only be approximately determined as the ions always have an energy distribution connected to the distribution of the position, so that only  $\text{TOF}(\overline{E}_{\text{kin}})$  can be measured. The probably best (and still experimentally feasible) approximation of the true distribution would be achieved by directly varying the average potential of the preparation ion trap instead of an element in some distance to the trap, but as it was anticipated to vary the energy by more than 100 eV, the potential  $V_{\text{PDT-low}}$  has been used instead to produce the wanted approximation of  $\text{TOF}(\overline{E}_{\text{kin}})$  due to present technical limitations of the trap potentials.

In Figure 7 a) an example of the  $\text{TOF}(\overline{E}_{\text{kin}})$  distribution yielding only moderate resolving powers of  $R_m \approx 200,000$  at best suitable energy is shown. In the central 100 eV region of the nearly parabolic profile, *i.e.* between the average kinetic energies  $\overline{E}_{\text{kin}} = 2425$  eV and 2525 eV, the TOF varies by at about 50 ns. Regarding the measured TOF for lower mean kinetic energies, it becomes obvious that the flight path (and time) for this energy

should be somewhat shortened in order to reach better equality with ions at higher kinetic energies. This was accomplished by raising the potential of one of the inner mirror electrodes at the beginning of the reflection region, so that the effect on the flight path is stronger for low-energy ions than for ions at higher energies.

The curve in Fig. 7 b) is the result of the same measurement after raising the potential  $V_{\text{EjM5}}$  of the 5th mirror electrode on the ejection side by 30 V, followed by a refocusing procedure using the strongly negative potential  $V_{\text{EjL}}$  to compensate the unavoidable change on the focal length of the system. The shape is significantly different and the region of flat response has been expanded. Within 100 eV energy width the TOF varies only by about 20 ns, while the imprinted (correlated) energy distribution of the ion cloud is estimated to remain below 40 eV (estimation by simulations with different cloud sizes and ejection fields in the Paul trap). This setting results in a better quality with already  $R_m > 500\,000$  at best suitable energy, and turned out to provide a useful initial configuration for the later fine tuning of the mirror voltages.

The fine tuning was done by respecting the unavoidable change of focal length of the system when any voltage is modified. When the system is already tuned so that a first-order TOF focus is present at the chosen number of laps, then a significant change of a single voltage (to modify the potential shape) will detune this focus. In this situation, it cannot be known immediately if this change would enable to find a better or worse TOF focus. It is thus necessary to either change the number of laps in order to search for the new focal length, or to use another electrode not involved in the region of ion reflection (*e.g.* central drift tube, negative lens electrode, or front-end electrodes between trap and MRTOF-MS) to re-adjust the focal length of the system.

In this work the negative lens electrode at ejection side has been used to recover the TOF focus for the same number of laps after changing a mirror potential in the ion-reflection region. Although this lens electrode influences the lateral focusing of ions and is mainly responsible for ion confinement, the response is weak enough to allow for larger voltage changes without harming the confinement. Furthermore, the change at such an electrode (far lower voltage than ion-reflection region) has only marginal influence on the  $\text{TOF}(E_{\text{kin}})$  profile, as the energy distribution within the ion cloud relative to the total kinetic energy, while passing this region, is very small. In this way, the potentials  $V_{\text{EjM1c},2,3,4,5}$  have been changed in (typically) 2–10 V steps, to chose a new shape in the reflection region, followed by the refocusing procedure before the resolving power has been determined for each setting.

As a benchmark for the efforts, stable  $^{36,40}\text{Ar}^+$  ions and also  $^{84}\text{Kr}^+$  have been delivered from the gas cell and accumulated in the linear Paul trap at the gas-cell side of the trap chamber. Traces of these noble-gas ions are present in the helium gas as contaminants and were ion-

ized by an  $\alpha$ -emitter source radiating into the gas. At the same time, reference alkali ions have been produced from the commercial ion source at the other side of the trap chamber, where  $^{39,41}\text{K}^+$  was used for  $m/q \approx 40$ , and  $^{85}\text{Rb}^+$  for  $m/q \approx 85$ . Time-of-flight spectra have been measured using the concomitant referencing mode, and were analyzed with an advanced code for software-based drift correction, which allows to compensate TOF drifts in short real-time intervals (as low as 1 s). The reference alkali ions have been used to perform the software drift correction for the analyte ions from the gas cell. Independent of the rate of ions delivered from the gas cell, the rate of reference ions was always tuned to be about one ion per cycle in average, which means 20 ions/s according to 50 ms duration for both subcycles together (analyte and reference cycle). Each pair of spectra (gas-cell ion spectrum, alkali ion spectrum) has been recorded for one hour and with high number statistics to obtain a robust estimation of the mass resolving power. The resulting TOF spectra have been fitted by a Johnson SU distribution [48, 49] capable to fit symmetric as well as skewed peak shapes.

The results show a stable performance for longer measurements yielding high mass resolving powers for the spectral pairs of  $R_m = 1.20(4) \cdot 10^6$  for  $^{36}\text{Ar}^+$  ( $1.00(3) \cdot 10^6$  for  $^{39}\text{K}^+$ ),  $R_m = 1.02(5) \cdot 10^6$  for  $^{40}\text{Ar}^+$  ( $1.04(4) \cdot 10^6$  for  $^{39}\text{K}^+$ ), and  $R_m = 0.93(4) \cdot 10^6$  for  $^{84}\text{Kr}^+$  ( $0.85(3) \cdot 10^6$  for  $^{85}\text{Rb}^+$ ). According to the recent works from other re-

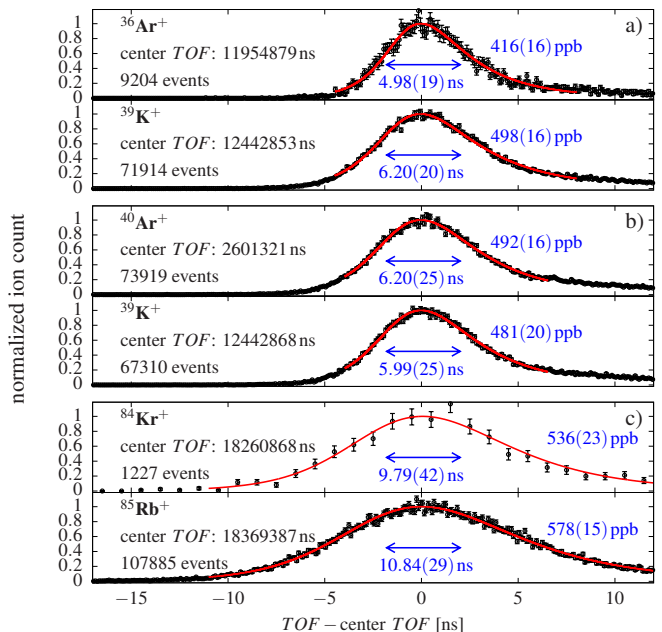


FIG. 8. a) Time-of-flight spectra measured in pairs (analyte/reference) for one hour accumulation time. a)  $^{36}\text{Ar}^+$  from the gas cell with  $^{39}\text{K}^+$  ions as reference yielding  $R_m \approx 1\,200\,000$ . b)  $^{40}\text{Ar}^+$  from the gas cell with  $^{39}\text{K}^+$  ions as reference yielding  $R_m \approx 1\,000\,000$ . c)  $^{84}\text{Kr}^+$  from the gas cell with  $^{85}\text{Rb}^+$  ions as reference yielding  $R_m \approx 900\,000$  (see text for the full number set).



search groups discussing particularly high resolving powers (see *e.g.* [50, 51]), and to the present knowledge of the authors, this is a new record for MRTOF mass spectrometry considering the long measurement time and high number statistics of ions in the spectra. This new achievement will facilitate mass measurements of nuclear isomeric states in future, where  $R_m \approx 10^6$  enables the identification of nuclear isomers (at FWHM level) with excitation energies of, for example, 38 keV for  $A/q \approx 40$ , 93 keV for  $A/q \approx 100$ , and 186 keV for  $A/q \approx 200$ . This performance is especially helpful for the separation of short-lived isomers by their mass value to identify ground state and isomeric state of nuclides for which the assignment is presently unknown (see *e.g.*  $^{78}\text{Y}$  with an isomer of 54 ms half life [52, 53]). With the high resolving power achieved for short measurement times as presented in this work, the MRTOF method has become competitive with the successful phase-imaging ion-cyclotron-resonance (PI-ICR) technique performed in Penning-trap experiments since 2013 [54, 55]. For PI-ICR, a 40-fold resolving power has been achieved as compared to the previously used TOF-ICR technique [56], which enables mass resolving powers around  $R_m \approx 1\,000\,000$  for 20 ms measurement time for Penning traps (for similar ion species discussed in this work).

#### IV. ONLINE EXPERIMENTS

In 2020 the MRTOF system was coupled to the new cryogenic gas cell and was transported to operate behind the ZeroDegree spectrometer, where continuous optimization and tests of the combined system were carried out. The system was ready to operate on-line just before the start of the 2020 winter campaign of in-beam  $\gamma$ -ray experiments [57, 58] of the new HiCARI project [59, 60], which enabled the first on-line commissioning of the new ZD-MRTOF setup in parasitic operation. Radioisotopes were produced by in-flight fission of a uranium beam from RIKEN's superconducting ring cyclotron (SRC) accelerator with a beam energy of 345 MeV/u (u as the atomic mass unit). The major production took place in the primary Beryllium target of 5 – 11 mm thickness, depending on the isotopes requested. The reaction products were separated by the BigRIPS separator and selectively forwarded to the HiCARI detector array. After passing the secondary reaction target and detectors, the reaction products were transported through the ZeroDegree spectrometer and stopped in the gas cell, whereas otherwise a lead beam dump would stop the radioisotopes without further usage. Energy degraders were employed to reduce the beam energy and to match the stopping power of the helium gas. The stopped reaction products were extracted mostly as singly-charged ions and molecular sidebands of the radioisotopes and other molecules ionized in the helium gas. The ions were transported to the MRTOF setup, where after applying the CGIMS scheme introduced in Sec. II B the isotope masses were

determined with high precision and accuracy. The 2020 HiCARI campaign lasted throughout the month November with five separate experiments of the project, and another two experiments took place in December. During our commissioning run, mass measurements covering four different regions in the nuclide chart have been carried out (see Fig 9).

The total system efficiencies were determined by comparing the incoming rate in front of the gas cell (within the PID system of RIBF) with the detected ion rate at the TOF detector. During the different runs performed, the system efficiency varied according to the presence of contaminants in the helium gas during this first on-line test. While some of the radioactive species were dispersed across molecular sidebands (*e.g.*  $^{55}\text{ScOH}^+$  with efficiency of less than  $10^{-4}$ ), very reasonable ion transport could be reached for many other species, *e.g.*  $^{85}\text{As}^+$  with 0.16 % and  $^{137}\text{Te}^+$  with 1.3 % total system efficiency.

A major mission of the commissioning was the test of components using true on-line beam. Nevertheless, the commissioning was highly successful for the study of nuclear masses with more than 70 atomic masses measured during the campaign. Around neutron-rich Ti and V isotopes, our results include isotopes from Sc to Fe with  $^{55}\text{Sc}$ ,  $^{58}\text{Ti}$ , and  $^{59}\text{V}$  being the most exotic ones measured in this region, which improve nuclear masses recently measured using the TOF-B $\rho$  method at NSCL [62] and RIBF [63] being the forefront of nuclear mass studies in this region. In the neutron-rich region above Ni, nuclides have been studied reaching from Ga to Kr with  $^{84}\text{Ga}$ ,  $^{86}\text{Ge}$ ,  $^{89}\text{As}$ , and  $^{91}\text{Se}$  as most exotic species. Among those isotopes,  $^{88,89}\text{As}$  have been measured for the first time while three other mass values provide a significant improvement of the previously performed measurements. Another region addressed with success is from Mo to Rh isotopes including the first mass measurement of  $^{112}\text{Mo}$ . In the fourth region addressed, *i.e.* near  $^{132}\text{Sn}$ , the sep-

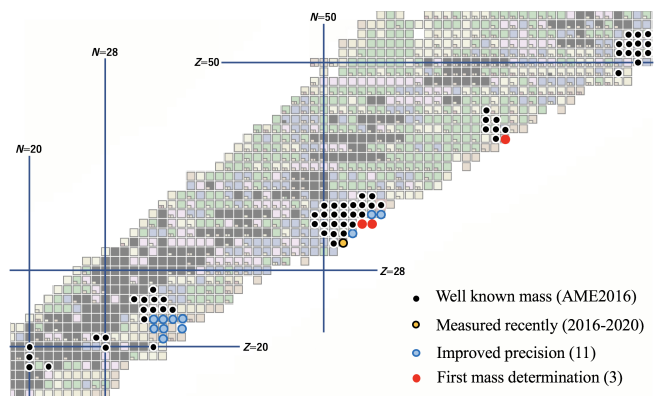


FIG. 9. Nuclear mass measurements during parasitic operation and the results by the ZD-MRTOF system (adapted from [61]). Background color code illustrates the measured precision from AME (see Nucleus-win for reference).

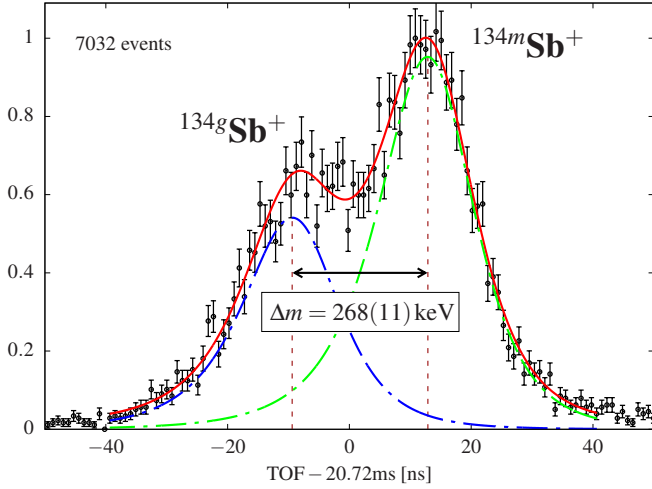


FIG. 10. Identification of nuclear ground state and isomeric state of  $^{134}\text{Sb}^+$  with a resolving power of  $R_m = 550\,000$  achieved prior to the most recent optimization.

aration of the ground state and the isomeric states of  $^{134g,m}\text{Sb}$  has been demonstrated [64] reaching a resolving power of  $R_m = 5.5 \cdot 10^5$  at that time (see Fig. 10). We note that this time period was before carrying out the new tuning and measurements reported in Sec. III. The excitation energy of the isomer in  $^{134}\text{Sb}$  was measured to be  $\Delta E = 268(11)$  keV being in agreement with  $\Delta E = 279(1)$  keV in the literature [65]. In total, three isotope masses have been measured for the first time and eleven other isotope masses improve the presently known uncertainty of AME2020 [52, 53] significantly. The data is presently under evaluation and will be discussed in separate dedicated frameworks.

Various different stable ion species, well-known radioactive ion species, and molecular ions were available as isobars throughout the online measurements for most of the observed spectra. This rich data set allowed to make a first study the of accuracy of the mass measurements along with the observation of unknown (or not well known) radioactive ion species. In Fig. 11 a mass evaluation of twenty different ion species with mass numbers 82-91 is shown. As presently only isobaric mass calibration is used systematic (mass dependent) effects become negligible, and in this analysis the uncertainties of the TOF measurements are assumed to purely depend on the total counting statistics of analyte and reference ions. The isobaric reference ions used for the measurement at each mass number (listed from lower to higher mass number):  $^{82-84}\text{Kr}^+$ ,  $^{84}\text{Kr}^{12}\text{H}^+$ ,  $^{86}\text{Kr}^+$ ,  $^{86}\text{Kr}^{12}\text{H}^+$ ,  $^{12}\text{C}_3\text{H}^{16}\text{O}_2\text{F}^+$ ,  $^{89}\text{Rb}^+$ ,  $^{90}\text{Kr}^+$ ,  $^{79}\text{Br}^{12}\text{C}^+$ . Unstable ions like  $^{90}\text{Kr}^+$  are part of the on-line beam.

For this data set of twenty different ion species, the weighted mean deviation of the measured masses from the AME2020 data is as low as  $2.26(0.80)$  keV, and the weighted mean relative mass deviation yields  $\delta m/m = 2.80(99) \times 10^{-8}$ . However, a more accurate study of

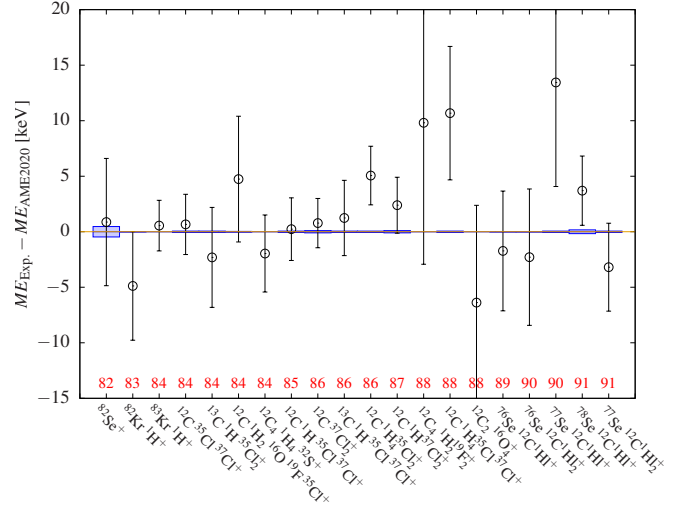


FIG. 11. Study of the mass accuracy using singly-charged isobaric ions from time-of-flight spectra at mass numbers 82-91. Each data point denotes an independent mass measurement using a reference species of same mass number. Blue bars: uncertainty of the ion species derived from the data in AME2020. Red numbers: atomic mass number of the ion species.

the accuracy limits requires separate measurements with higher statistics and will be performed in off-line conditions.

## V. SUMMARY

The new multi-reflection time-of-flight experiment for nuclear mass measurements downstream of the ZeroDegree spectrometer of RIKEN's BigRIPS facility has been introduced and relevant technical details have been discussed. An alternative in-MRTOF ion cleaning scheme has been introduced and was applied in on-line experiments. For the optimization procedure of the MRTOF ion mirrors, a useful method has been introduced which exploits the capability of a pulsed drift tube located in the transfer section of the system. Using the pulsed drift tube, the response of the time-of-flight for a wide energy range could be measured and provided a clear response to the modification of ion mirror voltages. This way of tuning followed by a thoughtful fine-tuning procedure enabled mass resolving powers exceeding  $R_m = 1\,000\,000$ , which is a mile stone for multi-reflection systems and has been demonstrated using measurement accumulation times of one hour and high ion count statistics. In 2020 the new setup has been coupled to a cryogenic gas cell and been commissioned on-line with parasitic radioisotope beams within the HiCARI project for in-beam  $\gamma$ -ray spectroscopy. During this on-line commissioning period, crucial tests of the new system could be undertaken and the readiness of the setup allowed to perform nu-

clear mass measurements of more than 70 different isotopes, where improvements of the previously known mass values have been achieved as well as newly measured masses. The setup is being improved continuously and high-precision nuclear mass measurements of exotic isotopes are planned to be performed on regular bases for the upcoming years.

## VI. ACKNOWLEDGEMENTS

We express our gratitude to the RIKEN Nishina Center for Accelerator-based Science, the Center for Nuclear Science at Tokyo University, and the HiCARI collaboration for their support of the online measurements. This work was supported by the Japan Society for the Promotion of Science KAKENHI (Grants No. 2200823, No. 24224008, No. 24740142, No. 15H02096, No. 15K05116, No. 17H01081, No. 17H06090, No. 18K13573, No. 19K14750, and 20H05648), and the RIKEN programme for Evolution of Matter in the Universe (r-EMU).

- 
- [1] H. Wollnik and M. Przewloka, *Int. J. Mass Spectrom. Ion Proc.* **96**, 267 (1990).
  - [2] R. Wolf, D. Beck, K. Blaum, C. Böhm, C. Borgmann, M. Breitenfeldt, F. Herfurth, A. Herlert, M. Kowalska, S. Kreim, D. Lunney, S. Naimi, D. Neidherr, M. Rosenbusch, L. Schweikhard, J. Stanja, F. Wienholtz, and K. Zuber, *Nucl. Instr. Meth. A* **686**, 82 (2012).
  - [3] R. N. Wolf, D. Beck, K. Blaum, C. Böhm, C. Borgmann, M. Breitenfeldt, N. Chamel, S. Goriely, F. Herfurth, M. Kowalska, S. Kreim, D. Lunney, V. Manea, E. Minaya Ramirez, S. Naimi, D. Neidherr, M. Rosenbusch, L. Schweikhard, J. Stanja, F. Wienholtz, and K. Zuber, *Phys. Rev. Lett.* **110**, 041101 (2013).
  - [4] P. Schury, M. Wada, Y. Ito, D. Kaji, F. Arai, M. McCormick, I. Murray, H. Haba, S. Jeong, S. Kimura, H. Koura, H. Miyatake, K. Morimoto, K. Morita, A. Ozawa, M. Rosenbusch, M. Reponen, P.-A. Söderström, A. Takamine, T. Tanaka, and H. Wollnik, *Phys. Rev. C* **95**, 011305 (2017).
  - [5] S. Ayet San Andrés, C. Hornung, J. Ebert, W. R. Plaß, T. Dickel, H. Geissel, C. Scheidenberger, J. Bergmann, F. Greiner, E. Haettner, C. Jesch, W. Lippert, I. Mardor, I. Miskun, Z. Patyk, S. Pietri, A. Pihkteleev, S. Purushothaman, M. P. Reiter, A.-K. Rink, H. Weick, M. I. Yavor, S. Bagchi, V. Charviakova, P. Constantin, M. Diwisch, A. Finlay, S. Kaur, R. Knöbel, J. Lang, B. Mei, I. D. Moore, J.-H. Otto, I. Pohjalainen, A. Prochazka, C. Rappold, M. Takechi, Y. K. Tanaka, J. S. Winfield, and X. Xu, *Phys. Rev. C* **99**, 064313 (2019).
  - [6] F. Wienholtz, D. Beck, K. Blaum, C. Borgmann, M. Breitenfeldt, R. B. Cakirli, S. George, F. Herfurth, J. D. Holt, M. Kowalska, S. Kreim, D. Lunney, V. Manea, J. Menéndez, D. Neidherr, M. Rosenbusch, L. Schweikhard, A. Schwenk, J. Simonis, J. Stanja, R. N. Wolf, and K. Zuber, *Nature* **498**, 346 (2013).
  - [7] M. Rosenbusch, P. Ascher, D. Atanasov, C. Barbieri, D. Beck, K. Blaum, C. Borgmann, M. Breitenfeldt, R. B. Cakirli, A. Cipollone, S. George, F. Herfurth, M. Kowalska, S. Kreim, D. Lunney, V. Manea, P. Navrátil, D. Neidherr, L. Schweikhard, V. Somà, J. Stanja, F. Wienholtz, R. N. Wolf, and K. Zuber, *Phys. Rev. Lett.* **114**, 202501 (2015).
  - [8] M. Rosenbusch, P. Ascher, D. Atanasov, C. Barbieri, D. Beck, K. Blaum, C. Borgmann, M. Breitenfeldt, R. B. Cakirli, A. Cipollone, S. George, F. Herfurth, M. Kowalska, S. Kreim, D. Lunney, V. Manea, P. Navrátil, D. Neidherr, L. Schweikhard, V. Somà, J. Stanja, F. Wienholtz, R. N. Wolf, and K. Zuber, *Phys. Rev. Lett.* **114**, 202501 (2015).
  - [9] A. Welker, N. A. S. Althubiti, D. Atanasov, K. Blaum, T. E. Cocolios, F. Herfurth, S. Kreim, D. Lunney, V. Manea, M. Mougeot, D. Neidherr, F. Nowacki, A. Poves, M. Rosenbusch, L. Schweikhard, F. Wienholtz, R. N. Wolf, and K. Zuber, *Phys. Rev. Lett.* **119**, 192502 (2017).
  - [10] Y. Ito, P. Schury, M. Wada, F. Arai, H. Haba, Y. Hirayama, S. Ishizawa, D. Kaji, S. Kimura, H. Koura, M. McCormick, H. Miyatake, J. Y. Moon, K. Morimoto, K. Morita, M. Mukai, I. Murray, T. Niwase, K. Okada, A. Ozawa, M. Rosenbusch, A. Takamine, T. Tanaka, Y. X. Watanabe, H. Wollnik, and S. Yamaki, *Phys. Rev. Lett.* **120**, 152501 (2018).
  - [11] E. Leistenschneider, M. P. Reiter, S. Ayet San Andrés, B. Kootte, J. D. Holt, P. Navrátil, C. Babcock, C. Barbieri, B. R. Barquest, J. Bergmann, J. Bollig, T. Brunner, E. Dunling, A. Finlay, H. Geissel, L. Graham, F. Greiner, H. Hergert, C. Hornung, C. Jesch, R. Klawitter, Y. Lan, D. Lascar, K. G. Leach, W. Lippert, J. E. McKay, S. F. Paul, A. Schwenk, D. Short, J. Simonis, V. Somà, R. Steinbrügge, S. R. Stroberg, R. Thompson, M. E. Wieser, C. Will, M. Yavor, C. Andreoiu, T. Dickel, I. Dillmann, G. Gwinner, W. R. Plaß, C. Scheidenberger, A. A. Kwiatkowski, and J. Dilling, *Phys. Rev. Lett.* **120**, 062503 (2018).
  - [12] P. Schury, T. Niwase, M. Wada, P. Brionnet, S. Chen, T. Hashimoto, H. Haba, Y. Hirayama, D. S. Hou, S. Iimura, H. Ishiyama, S. Ishizawa, Y. Ito, D. Kaji, S. Kimura, H. Koura, J. J. Liu, H. Miyatake, J.-Y. Moon, K. Morimoto, K. Morita, D. Nagae, M. Rosenbusch, A. Takamine, Y. X. Watanabe, H. Wollnik, W. Xian, and S. X. Yan, *Phys. Rev. C* **104**, L021304 (2021).
  - [13] Y. Ishida, M. Wada, and H. Wollnik, *Nucl. Instrum. Meth. B* **241**, 983 (2005).
  - [14] P. Schury, M. Wada, Y. Ito, F. Arai, S. Naimi, T. Sonoda, H. Wollnik, V. Shchepunov, C. Smorra, and C. Yuan, *Nucl. Instr. Meth. B* **335**, 39 (2014).
  - [15] W. R. Plaß, T. Dickel, U. Czok, H. Geissel, M. Petrick, K. Reinheimer, C. Scheidenberger, and M. I. Yavor, *Nucl. Instr. Meth. B* **266**, 4560 (2008).
  - [16] W. Plaß, T. Dickel, S. Purushothaman, P. Dendooven, H. Geissel, J. Ebert, E. Haettner, C. Jesch, M. Ranjan, M. Reiter, H. Weick, F. Amjad, S. Ayet, M. Di-

- wisch, A. Estrade, F. Farinon, F. Greiner, N. Kalantar-Nayestanaki, R. Knöbel, J. Kurcewicz, J. Lang, I. Moore, I. Mukha, C. Nociforo, M. Petrick, M. Pfützner, S. Pietri, A. Prochazka, A.-K. Rink, S. Rinta-Antila, D. Schäfer, C. Scheidenberger, M. Takechi, Y. Tanaka, J. Winfield, and M. Yavor, *Nucl. Instr. Meth. B* **317**, 457 (2013).
- [17] C. Jesch, T. Dickel, W. R. Plaß, D. Short, S. A. S. Andres, J. Dilling, H. Geissel, F. Greiner, J. Lang, K. G. Leach, W. Lippert, C. Scheidenberger, and M. I. Yavor, in *TCP 2014*, edited by M. Wada, P. Schury, and Y. Ichikawa (Cham, 2017) pp. 175–184.
- [18] T. Y. Hirsh, N. Paul, M. Burkey, A. Aprahamian, F. Buchinger, S. Caldwell, J. A. Clark, A. F. Levand, L. L. Ying, S. T. Marley, G. E. Morgan, A. Nystrom, R. Orford, A. P. Galván, J. Rohrer, G. Savard, K. S. Sharma, and K. Siegl, *Nucl. Instrum. Meth. B* **376**, 229 (2016).
- [19] B. Schultz, J. Kelly, C. Nicoloff, J. Long, S. Ryan, and M. Brodeur, *Nucl. Instrum. Meth. B* **376**, 251 (2016).
- [20] P. Chauveau, P. Delahaye, G. D. France, S. E. Abir, J. Lory, Y. Merrer, M. Rosenbusch, L. Schweikhard, and R. Wolf, *Nucl. Instr. Meth. B* **376**, 211 (2016).
- [21] J.-Y. Wang, Y.-L. Tian, Y.-S. Wang, Z.-G. Gan, X.-H. Zhou, H.-S. Xu, and W.-X. Huang, *Nucl. Instrum. Meth. B* **463**, 179 (2020).
- [22] K. Murray, J. Dilling, R. Gornea, Y. Ito, T. Koffas, A. A. Kwiatkowski, Y. Lan, M. P. Reiter, V. Varentsov, T. Brunner, and w. t. n. collaboration, *Hyperfine Interactions* **240**, 97 (2019).
- [23] M. Rosenbusch, M. Wada, P. Schury, Y. Ito, H. Ishiyama, S. Ishizawa, Y. Hirayama, S. Kimura, T. Kojima, H. Miyatake, J. Moon, T. Niwase, T. Sonoda, A. Takamine, Y. Watanabe, and H. Wollnik, *Nucl. Instrum. Meth. B* **463**, 184 (2020).
- [24] H. Sakurai, *AIP Conf. Proc.* **1269**, 84 (2010).
- [25] H. Okuno, N. Fukunishi, and O. Kamigaito, *Prog. Theo. Exp. Phys.* **2012** (2012).
- [26] T. Kubo, D. Kameda, H. Suzuki, N. Fukuda, H. Takeda, Y. Yanagisawa, M. Ohtake, K. Kusaka, K. Yoshida, N. Inabe, T. Ohnishi, A. Yoshida, K. Tanaka, and Y. Mizoi, *Prog. Theo. Exp. Phys.* **2012** (2012).
- [27] H. Wollnik and A. Casares, *Int. J. Mass Spectrom.* **227**, 217 (2003).
- [28] R. N. Wolf, G. Marx, M. Rosenbusch, and L. Schweikhard, *Int. J. Mass Spectrom.* **313**, 8 (2012).
- [29] J. T. Johnson, I. J. Carrick, G. S. Eakins, and S. A. McLuckey, *Analytical Chemistry* **91**, 8789 (2019).
- [30] Y. Toker, N. Altstein, O. Aviv, M. L. Rappaport, O. Heber, D. Schwalm, D. Strasser, and D. Zajfman, *J. Instrum.* **4**, P09001 (2009).
- [31] T. Dickel, W. Plaß, A. Becker, U. Czok, H. Geissel, E. Haettner, C. Jesch, W. Kinsel, M. Petrick, C. Scheidenberger, A. Simon, and M. Yavor, *Nucl. Instrum. Meth. A* **777**, 172 (2015).
- [32] P. Fischer, S. Knauer, G. Marx, and L. Schweikhard, *Rev. Sci. Instrum.* **89**, 015114 (2018).
- [33] F. Wienholtz, S. Kreim, M. Rosenbusch, L. Schweikhard, and R. Wolf, *Int. J. Mass Spectrom.* **421**, 285 (2017).
- [34] D. Steppenbeck *et al.*, *Nature* **502**, 207 (2013).
- [35] P. Schury, Y. Ito, M. Wada, and H. Wollnik, *Int. J. Mass Spectrom.* **359**, 19 (2014).
- [36] A. Takamine, S. Iimura, D. Hou, M. Wada, M. Rosenbusch, S. Chen, W. Xian, S. Yan, S. P., Y. Ito, M. Kojima, T. Sonoda, Y. X. Watanabe, H. Ueno, and H. Ishiyama, *RIKEN Acc. Prog. Rep.* **54** (2020).
- [37] S. Iimura, A. Takamine, D. Hou, Rosenbusch, M. Wada, S. Chen, J. Liu, W. M. Xian, S. Yan, S. P., S. Kimura, T. Niwase, Y. Ito, T. Sonoda, M. Kojima, Y. X. Watanabe, S. Naimi, S. Michimasa, S. Nishimura, A. Odahara, and H. Ishiyama, *RIKEN Acc. Prog. Rep.* **55** (2021).
- [38] G. Savard, J. Clark, C. Boudreau, F. Buchinger, J. Crawford, H. Geissel, J. Greene, S. Gulick, A. Heinz, J. Lee, A. Levand, M. Maier, G. Münzenberg, C. Scheidenberger, D. Seweryniak, K. Sharma, G. Sprouse, J. Vaz, J. Wang, B. Zabransky, and Z. Zhou, *Nucl. Instrum. Meth. B* **204**, 582 (2003).
- [39] L. Weissman, P. Lofy, D. Davies, D. Morrissey, P. Schury, S. Schwarz, T. Sun, and G. Bollen, *Nucl. Phys. A* **746**, 655 (2004).
- [40] M. Wada, *Nucl. Instrum. Meth. B* **317**, 450 (2013).
- [41] T. Dickel, W. Plaß, H. Geissel, F. Heiße, I. Miskun, S. Purushothman, M. Reiter, A.-K. Rink, and C. Scheidenberger, *Nucl. Instrum. Meth. B* **376**, 216 (2016).
- [42] C. Sumithrarachchi, D. Morrissey, S. Schwarz, K. Lund, G. Bollen, R. Ringle, G. Savard, and A. Villari, *Nucl. Instrum. Meth. B* **463**, 305 (2020).
- [43] P. Schury, Y. Ito, M. Rosenbusch, H. Miyatake, M. Wada, and H. Wollnik, *Int. J. Mass Spectrom.* **433**, 40 (2018).
- [44] F. Wienholtz, K. Blaum, J. Karthein, D. Lunney, S. Malbrunot-Ettenauer, V. Manea, M. Mougeot, L. Schweikhard, T. Steinsberger, and R. Wolf, *Nucl. Instrum. Meth. B* **463**, 348 (2020).
- [45] P. Fischer and L. Schweikhard, *Rev. Sci. Instrum.* **92**, 063203 (2021).
- [46] P. Schury, M. Wada, H. Wollnik, J.-Y. Moon, T. Hashimoto, and M. Rosenbusch, *Rev. Sci. Instr.* **91**, 014702 (2020).
- [47] H. Wollnik, *J. Mass Spectrom.* **34**, 991 (1999).
- [48] N. L. Johnson, *Biometrika* **36**, 149 (1949).
- [49] N. L. Johnson, *Biometrika* **36**, 297 (1949).
- [50] M. I. Yavor, T. V. Pomozev, S. N. Kirillov, Y. I. Khasin, and A. N. Verenchikov, *Int. J. Mass Spectrom.* **426**, 1 (2018).
- [51] I. Mardor, S. A. S. Andrés, T. Dickel, D. Amanbayev, S. Beck, J. Bergmann, H. Geissel, L. Gröf, E. Haettner, C. Hornung, N. Kalantar-Nayestanaki, G. Kripko-Koncz, I. Miskun, A. Mollaebrahimi, W. R. Plaß, C. Scheidenberger, H. Weick, S. Bagchi, D. L. Balabanski, A. A. Bezbakh, Z. Brencic, O. Charviakova, V. Chudoba, P. Constantin, M. Dehghan, A. S. Fomichev, L. V. Grigorenko, O. Hall, M. N. Harakeh, J.-P. Hucka, A. Kankainen, O. Kiselev, R. Knöbel, D. A. Kostyleva, S. A. Krupko, N. Kurkova, N. Kuzminchuk, I. Mukha, I. A. Muzalevskii, D. Nichita, C. Nociforo, Z. Patyk, M. Pfützner, S. Pietri, S. Purushothaman, M. P. Reiter, H. Roesch, F. Schirru, P. G. Sharov, A. Spătaru, G. Stanic, A. State, Y. K. Tanaka, M. Vencelj, M. I. Yavor, and J. Zhao, *Phys. Rev. C* **103**, 034319 (2021).
- [52] W. Huang, M. Wang, F. Kondev, G. Audi, and S. Naimi, *Chinese Physics C* **45**, 030002 (2021).
- [53] M. Wang, W. Huang, F. Kondev, G. Audi, and S. Naimi, *Chinese Physics C* **45**, 030003 (2021).
- [54] S. Eliseev, K. Blaum, M. Block, C. Droese, M. Goncharov, E. Minaya Ramirez, D. A. Nesterenko, Y. N. Novikov, and L. Schweikhard, *Phys. Rev. Lett.* **110**, 082501 (2013).
- [55] M. Block, *Nucl. Instrum. Meth. B* **376**, 265 (2016).



- [56] M. König, G. Bollen, H.-J. Kluge, T. Otto, and J. Szerypo, *Int. J. Mass Spectrom. Ion Proc.* **142**, 95 (1995).
- [57] P. Doornenbal, *Progress of Theoretical and Experimental Physics* **2012** (2012).
- [58] P. Doornenbal, *AIP Conf. Proc.* **1753**, 070002 (2016).
- [59] K. Wimmer, P. Doornenbal, N. Aoi, H. Baba, F. Browne, P. Campell, H. Crawford, H. De Witte, C. Fransen, H. Hess, S. Iwazaki, J. Kim, A. Kohda, T. Koiwai, B. Mauss, B. Moon, T. Parry, P. Reiter, D. Suzuki, R. Taniuchi, S. Thiel, and Y. Yamamoto, *RIKEN Acc. Prog. Rep.* **54** (2021).
- [60] P. Doornenbal, K. Wimmer, N. Aoi, H. Baba, F. Browne, P. Campell, M. Carpenter, A. Corsi, M. L. Cortéz, H. Crawford, M. Cromaz, P. Fallon, A. Gillibert, H. Hess, E. Ideguchi, T. Isobe, V. Lapoux, H. Liu, A. Macchiavelli, M. Niikura, O. Möller, S. Nishimura, A. Obertelli, V. Panin, N. Pietralla, P. Reiter, L. Riley, H. Sakurai, M. Seidlitz, D. Suzuki, S. Thiel, V. Werner, N. Warr, and Y. Yamamoto, *RIKEN RIBF proposal Np1812-ribf173* (2018).
- [61] M. Rosenbusch, S. Chen, Y. Hirayama, D. Hou, S. Iimura, H. Ishiyama, Y. Ito, S. Kimura, J. Liu, S. Michimasa, H. Miyatake, S. Naimi, S. Nishimura, T. Niwase, S. P., A. Takamine, M. Wada, Y. X. Watanabe, H. Wollnik, W. Xian, and S. Yan, *RIKEN Acc. Prog. Rep.* **55** (2021).
- [62] Z. Meisel, S. George, S. Ahn, D. Bazin, B. A. Brown, J. Browne, J. F. Carpino, H. Chung, R. H. Cyburt, A. Estradé, M. Famiano, A. Gade, C. Langer, M. Matoš, W. Mittig, F. Montes, D. J. Morrissey, J. Pereira, H. Schatz, J. Schatz, M. Scott, D. Shapira, K. Smith, J. Stevens, W. Tan, O. Tarasov, S. Towers, K. Wimmer, J. R. Winkelbauer, J. Yurkon, and R. G. T. Zegers, *Phys. Rev. C* **101**, 052801 (2020).
- [63] S. Michimasa, M. Kobayashi, Y. Kiyokawa, S. Ota, R. Yokoyama, D. Nishimura, D. S. Ahn, H. Baba, G. P. A. Berg, M. Dozono, N. Fukuda, T. Furuno, E. Ideguchi, N. Inabe, T. Kawabata, S. Kawase, K. Kisamori, K. Kobayashi, T. Kubo, Y. Kubota, C. S. Lee, M. Matsushita, H. Miya, A. Mizukami, H. Nagakura, H. Oikawa, H. Sakai, Y. Shimizu, A. Stolz, H. Suzuki, M. Takaki, H. Takeda, S. Takeuchi, H. Tokieda, T. Uesaka, K. Yako, Y. Yamaguchi, Y. Yanagisawa, K. Yoshida, and S. Shimoura, *Phys. Rev. Lett.* **125**, 122501 (2020).
- [64] W. Xian, M. Rosenbusch, S. Chen, Y. Hirayama, D. Hou, S. Iimura, H. Ishiyama, Y. Ito, S. Kimura, J. Liu, H. Miyatake, S. Nishimura, S. P., A. Takamine, M. Wada, Y. X. Watanabe, H. Wollnik, and S. Yan, *RIKEN Acc. Prog. Rep.* **55** (2021).
- [65] A. K. Jain, B. Maheshwari, S. Garg, M. Patial, and B. Singh, *Nuclear Data Sheets* **128**, 1 (2015).